ORIGINAL PAPER

Optimization of TIG welding process parameters on chrome alloy steel using Box–Behnken method

Bhiksha Gugulothu[1] · Srikanth Karumuri[2] · S. Vijayakumar[3] · B. Muthuvel[4] · Suresh Seetharaman[5] · S. Jeyakrishnan[6] · Kuldeep K. Saxena[7]

Abstract

Chrome steel is a quality high-carbon alloy steel that offers a high degree of hardness with compressive strength, abrasion resistance, good ductility relatively good impact properties at low temperatures. This paper aims to determine the best set of process parameters for TIG welding on chrome steel alloys (EN31 and AISI 52100) to achieve higher ultimate tensile strength (UTS) and hardness (BHN). Current (A: 150–200 A), weld speed (B: 2–4 mm/s), and electrode diameter (C: 2–3 mm) were used as input parameters for TIG welding process. The Box–Behnken method of the RSM approach was used to conduct the Design of Experiments (DoE). Analysis of variance (ANOVA) employs an arithmetical approach to determine the perfect amount of dependent variables to make best-designing limitations via confirmation readings. UTS and BHN values are observed from 225 to 321.5 MPa and 78.5 to 97.5 HV respectively. From the SN ratio response table, it is noticed that the optimal conditions for UTS are obtained at current-175 A (level 2), welds speed-4 m/s (level 3), and electrode diameter-2.5 mm (level 2) and the current is the main parameter to improve the UTS and BHN of the joint followed by weld speed and electrode diameter. Based on SEM analysis, it is been noted that the presence of voids in the weld pool can be attributed to the absorption of oxygen and nitrogen from the surrounding atmosphere as well as inadequate shielding gas. The primary cause of fracture is overload with the failure being predominantly influenced by the coalescence of microporosity.

Keywords Tungsten inert gas welding · Optimization · Mechanical behavior · Box–Behnken design · Welding parameters

1 Introduction

The preservation of austenite content in the microstructure has an important impact on the mechanical characteristics of hardened chrome steel, which include flexural strength, micro-hardness, and Young's modulus. The EN31 Alloy Steel is a low alloy steel that is primarily used for bearing applications. A high level of hardness, compressive strength, and abrasion resistance are all provided by the superb high-carbon alloy steel known as AISI 52100. Chrome steel is typically utilized extensively in the automotive industry for gear, shaft, pinion, camshaft and machining components as well as many other general engineering applications. Welding is a method of uniting a couple of metallic elements by melting solid components and applying an electrode to the molten metal's surface to establish a resilient bond. During

✉ S. Vijayakumar
    vijaysundarbe@gmail.com

1   Department of Mechanical Engineering, Bule Hora University, Post Box No-144, Oromia, Ethiopia

2   Department of Mechanical Engineering, College of Engineering and Technology, Mizan Tepi University, Tepi Campus, P.O. Box 121, Tepi, Ethiopia

3   Department of Mechanical Engineering, BVC Engineering College (Autonomous), Odalarevu, Andhra Pradesh 533210, India

4   Department of EEE, BVC Institute of Technology and Science, Amalapuram, Konaseema District, Andhra Pradesh, India

5   Department of Electrical and Electronics Engineering, KIT-Kalaignar Karunanidhi Institute of Technology, Coimbatore, India

6   Department of Mechanical Engineering, ARM College of Engineering and Technology, Maraimalainagar, Chennai 603209, India

7   Division of Research and Development, Lovely Professional University, Phagwara 144411, India

the TIG process, the arc heat is about 10,000 °C and shielding gases (Ar, He & Ni) and the mixing of any of two gases are utilized to avoid oxidization [1]. TIG welding has advantages over other welding techniques in terms of amperage and adaptability because it consumes less energy. It is useful for many applications such as the Manufacture of pressure vessels, steel assemblies, Automotive, and home development industries [2]. Wichan Chuaiphan et al. [3] studied the SEM and oxidization enactment of weld-metal by way of the tungsten inert gas approach. Dadfar et al. [4] investigated the corrosion performance of SS-316L plates joined through TIG weld at a physiological solution and the heat treatment result may improve behavior on resistance to bonded SS-316. Ravi Kant et al. [5] considered four factors to be working on weld processes which are pressure (p), rough mass flowing amount (Q), stand-off space, and traversing speediness. Kumar Sahu et al. [6] have done turning operation on EN-31 steel and three factors are considered for optimization work in which the depth of cut contributed (54%) more for Ti–Al–N cutting force followed by feed rate (36%), and, spindle speed (1.8%). MQL of vegetable oil and investigated cutting temperature at various distances of the nozzle in EN-31 turning task and cutting speed is more influenced variable by around 69% compared to feed rate. Humans and robots working together are most requirements in the manufacturing processes [7, 8]. Venkata Ramana et al. [9] did optimization work on dissimilar SS-304L/SS-430 joins made by Robotic TIG, Weld-current-180 A, electrode traveling rapidity of 0.08 mm/min and wire feed of 0.821 mm/min were identified to be optimal for maximizing the bearing strength (IS) in Taguchi-based optimization of divergent of SS-430 and SS-304L joints. Taguchi-RSM is a good way to improve the quality of dissimilar materials junctions by enhancing welding process parameters. Defects in welding is a common problems that happened due to inappropriate welding procedures, Welding current, electrode diameter, and duration of the weld etc. Radiography experimental test is used for checking interior defects of TIG welds [10]. Vijayakumar et al. [11] explained that analyze defects and behavior of SS 304 alloy on TIG through radiographic testing and destructive tests of tensile strength and hardness. Microstructure analysis [12, 13] of SS 316L metal joined on weld operation (TIG) by the addition of Al_2O_3 [14, 15].Tensile property has been improved on Al2219 welding by adjusting welding geometry such as penetration depth, width, thickness, and reinforcement height [16, 17].Taguchi and Box–Behnken are some of the optimization techniques used in many research works [18]. Optimal process factors for TIG welded 316 SS were noticed on mechanical properties at current-150 A, weld speed-190 mm/min and flow rate of gas-15 l/min [19–21]. The Taguchi technique is used to establish the optimization technique for the tungsten inert gas process parameter and examine the tensile strength of the welded joint made

of AISI 4140 stainless steel. To conduct the experiments utilizing the L9 orthogonal array, three distinct welding process parameters—welding current, welding speed, and filler diameter have been chosen. For Tungsten Inert Gas welding of AISI 4140 stainless steel plates, the regression model was employed to determine a link between welding input parameters. The findings of the ANOVA revealed that welding speed is the major factor in achieving tensile strength [22]. Exploring and standardizing microwave joining is crucial for its commercial viability. The use of microwave hybrid heating to join Inconel-625 has been studied by analyzing the effects of process parameters. The experiments were conducted under different conditions within a microwave applicator. The impact of varying process parameters on the melting of the joint interface was also analyzed [23]. Sekhon et al. [24] investigated the tool pin profile along with rotational and welding speed on the FSW performance on a joint of pure copper and brass and analyze the breaking load and percentage elongation. A study was conducted to create butt welded joints on austenitic stainless steel using three different levels of current, gas flow rate, and nozzle-to-workpiece distance. The experimental parameters were varied to investigate their effects on the welding process. In terms of the ultimate tensile strength of the welded specimens, the weld quality has been estimated [25]. The tensile properties of TIG welded joints in 2219-T8 alloy were improved by modifying the weld geometry through the use of multi-pass swing welding. Investigations were conducted to examine the impact of weld geometry on the joint's tensile strength. Additionally, an orthogonal experiment design was employed to optimize the geometry parameters. Adjusting the weld geometry resulted in the creation of joints with a tensile strength coefficient of 70% and elongation exceeding 4%. [26]. The above literature survey explained the development of mechanical properties of welded joint materials with suitable weld parameters on TIG welding. Box–Behnken designs are used to generate higher-order response surfaces, which can be achieved with fewer runs compared to the traditional factorial method. This technique involves suppressing certain runs to maintain the accuracy of the higher-order surface definition [27–30].

The above literature reviews discussed the Taguchi methodology only for TIG welding optimization and noticed that many researchers have selected the Taguchi method for design of experiment work and optimization. From this work, Box–Behnken Technique is implanted to identify the number of experiments, optimal factor levels and the understanding of the relationships between variables (current, weld speed, and electrode diameter) and the response (UTS and BHN). The novelty of this study lies in the utilization of TIG welding to join chrome steel alloys (EN31 and AISI 52100) under different combinations of input weld parameters. The mechanical properties, specifically Ultimate Tensile Strength (UTS) and Brinell Hardness Number (BHN), were

Table 1 Chemical composition of chrome steel alloys (in wt%)

Elements	Mn	C	Si	Mo	Cr	Fe
EN31 (%)	0.75	1.2	0.2	0.18	0.7	Balance
AISI 52100 (%)	0.45	0.9	0.15	0.25	1.3	Balance

Table 2 Mechanical properties of chrome steels

Materials	Tensile strength (MPa)	Yield strength (MPa)	Elongation, (%)	Hardness (HV)
EN31	650	420	26	195
AISI 52100	720	460	17	105

Fig. 1 TIG welding setup

analyzed and optimized using the Box–Behnken Technique. Compared to the central composite technique, this is one of the new optimization techniques in Response Surface Methodology (RSM) that aids in determining the optimal parameters for enhancing the UTS and hardness of welded chrome steel plates. The software used to determine the optimization results is Design Expert Software, which also examines the interaction between the input parameters. The main objective of the study was to optimize the TIG welding process parameters for chrome steel alloys to achieve higher UTS and BHN values, and the research findings provided insights into the effects of process parameters on the mechanical properties and microstructure of the welded joints.

2 Materials and methods

The chrome steel plates (EN31 and AISI 52100) with a cross-section of length (150 mm), Width (60 mm), and thickness (5 mm) are employed. The welding process is carried out by AC/DC 500P model TIG machine which has a capacity of current 400A along the inverter. Tungsten is used as electrode material. The chemical element and mechanical properties of Chrome steel (CS) alloy are displayed in Tables 1 and 2. The experimental setup for TIG Welding is depicted in Fig. 1. The initial step involves edge preparation of the experimental specimen, which ensures optimal fusion at the weld root with minimal weld metal. This is crucial for achieving complete welding penetration and minimizing distortion of the parts during the welding process. Acetone is used to remove any unwanted particles from the workpiece. The pair of work-pieces are then positioned on the bed and joined using a TIG welding machine. The cross-section area and samples of weld joints are presented in Fig. 2. Throughout the welding operation, the arc remains constant, with an arc-slit of 3 to 5 mm, keeping the electrode perpendicular to the preferred plates. TIG welding of CS is available, including information on current, welding speed, and electrode diameter. Current, A (Amp) is applied in the range of 150, 175, 200 A for each flux, weld speed, B is 2, 3, and 4 mm/min, and electrode diameters, C is 2, 2.4, and 3 mm correspondingly. Each factor in weld operation at different levels is also displayed in Table 3.

3 Box–Behnken design (BBD)

As per the Response Surface Methodology, there are different types of methods such as Box–Behnken design, Central composite design, Gradient-enhanced kriging (GEK), IOSO method. Box–Behnken Design is commonly used for fitting second-order polynomial models to optimize a response variable [31, 32]. It uses a reduced number of experimental runs compared to a full factorial design, making it more efficient when the number of experimental runs needs to be limited. This is particularly useful for situations where the relationship between the input factors and the output response is expected to be smooth and not too complex.
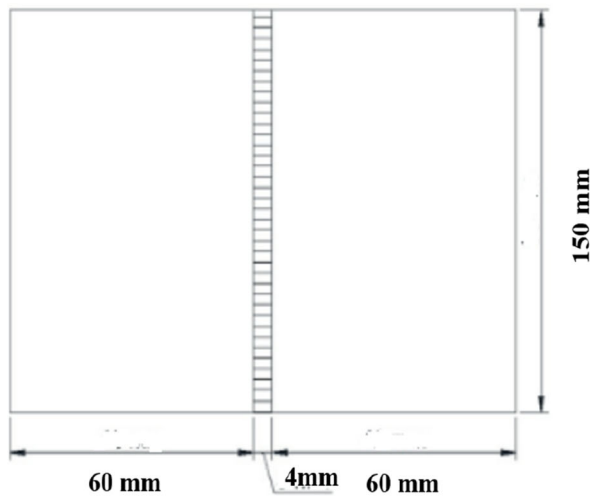
Fig. 2 TIG welded joint on chrome steel plates

Table 3 TIG factors and their levels

Parameter names	1st Level	2nd Level	3rd Level
A-Current (A)	150	175	200
B-weld speed (mm/min)	2	3	4
C-Electrode diameter (mm)	2	2.5	3

As per the Box–Behnken Design (BBD), the number of experiments is typically determined by the formula:

Number of Experiments $= (k + 1)^2$

where "k" is the number of factors being investigated, and the "+ 1" term is for the center point runs (used to estimate the pure error and lack-of-fit). Since BBD uses a combination of factorial points and center points to approximate the response surface, it requires a minimum of three levels for each factor: low, center, and high levels. With three levels per factor (k = 3), the minimum number of experiments would be (3 + 1)^2 = 16. However, one of these runs is typically replicated at the center point to estimate experimental error, leaving us with 15 unique experimental runs. This number allows them to obtain the necessary information to build a second-order polynomial model to optimize the response variable with a relatively efficient and balanced design.

As per ASTM D638 standard dimensions [33–35], the welded joints are cut for conducting the tensile test, the specimens for the tensile test are shown in Fig. 3. The measurement of hardness can be found by applying ball indenter at 500 g load with an interval of 10 s. Three readings are taken for each test and make their average value [36–38]. UTS and BHN readings for weld joints range from 225 to 321.5 MPa
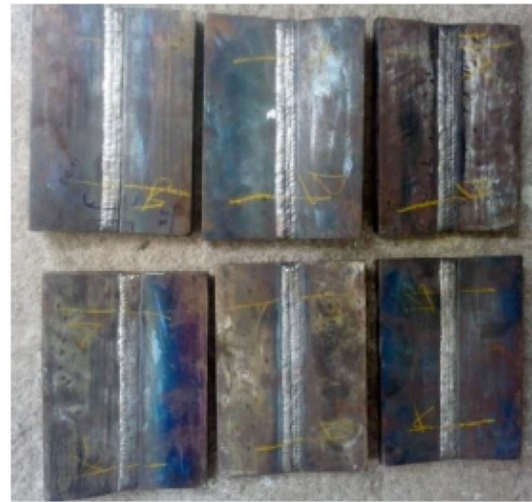

Fig. 3 Tensile test specimens as per ASTM D638

and 78.5 to 97.5 HV respectively which is shown in Table 4. The potential for UTS to increase as welding parameters such as weld current, speed, and electrode diameter is changed to connect prepared work pieces.

4 Result and discussions

During the experimental testing of hardness and tensile strength, the standard error ranged from 0.3536 to 1.174, with an average mean std error of 0.524 throughout the optimization procedure. The lowest combined UTs (225 MPa) are observed on run-5 (A-150 A, B-3 mm/min, and C-2 mm), while the highest amount 321.5 MPa was observed on Run-8 (A-175 A, B-3 mm/min, and C-2.4 mm). Similarly, the maximum & minimum micro HV are detected on experimental run-12 (A-175 A, B-2 mm/min, and C-3 mm) and Run-10 (A-150 A, B-2 mm/min, C-2.5 mm). Outputs Optimizations were measured from response optimum factors

Table 4 Observational result on UTS and BHN

Runs	A: Current (A)	B: Weld speed (m/s)	C: Electrode diameter (mm)	UTS (MPa)	Hardness, BHN (HV)
1	175	3	2.5	282.5	90
2	150	4	2.5	301.2	88.5
3	175	2	2	275	79
4	175	3	2.5	242.5	81.5
5	150	3	2	225	92
6	200	2	2.5	305.8	95
7	175	4	2	285.4	92.5
8	175	3	2.5	321.5	85
9	200	4	2.5	225.2	86.5
10	150	2	2.5	238	78.5
11	200	3	3	264	96
12	175	2	3	253.1	97.5
13	175	4	3	298.6	84
14	150	3	3	229	79.5
15	200	3	2	272.3	83

Table 5 ANOVA result for UTS

Sources	SS	D.F.	MS	F	p
Models	9081.76	9	1009.08	11.05	0.05081
A-Current	686.35	1	686.35	13.7122	0.04372
B-Weld speed	185.28	1	185.28	9.1923	0.06793
C-Electrode Diameter	21.13	1	21.13	0.0219	0.8881
A*B	5169.61	1	5169.61	5.36	0.0684
A*C	37.82	1	37.82	0.0392	0.8508
B*C	308.00	1	308.00	0.3196	0.5963
A*A	1874.77	1	1874.77	1.95	0.2219
B*B	231.41	1	231.41	0.2401	0.6449
C*C	536.87	1	536.87	0.5571	0.4890
Residual	4818.48	5	963.70		
Lack of Fit	1697.81	3	565.94	0.3627	0.7908
Pure Error	3120.67	2	1560.33		
Cor-Total	13,900.24	14			

using a Box–Behnken ramp solution, and produced values of UTS-267 MPa and BHN-86HV with input factors current of 191 Am, weld speed of 3.4 mm/min, and electrode diameter of 2.35 mm, with standard errors of 12.7 and 1.75, respectively and also found out standard Error (StdErr) for UTS-12.76 and BHN-1.76 in Fig. 5.

The result of the ultimate strength of ANOVA indicated that F 11.05 is the model indicated which is not important while assessment to noise. Due to noise, magnitude (F) had 50.81% possibility. Model terms are significant if their P values are less than 0.0500 [39–41]. The model terms are not significant if their values exceed 0.1000. The F value 0.36 for the Lack of Fit indicates that it is not noteworthy once

associated with the clean mistake. A momentous Lack of Fit F-value owing to noise 79.08 percent is more potential. Similarly, Table 4 specified for Hardness test on ANOVA. Tables 5 and 6 showed that the Fisher ratio (F) value was not more than 10 which means the ANOVA model is superb in both cases (UTS and BHN), and the combination of current and welding speed (A*B) is the most significant parameter in the experimental work to improve the mechanical properties of TIG welds. Figure 3 showed the interaction between weld speed and current on Ultimate tensile strength.it is exposed that UTS is increasing by increasing weld speed and current values. The rise in current at the point of contact under various circumstances might be responsible for the good strength

Table 6 ANOVA-BHN result

Sources	Sum of squares (SS)	Degree of freedom (DF)	Mean square (MS)	F-value	p value
Model	518.75	9	57.64	15.32	0.0402
A-Current	60.50	1	60.50	15.58	0.0445
B-Weld speed	0.2812	1	0.2812	13.0260	0.0783
C-Electrode diameter	13.78	1	13.78	1.27	0.3106
A × B	85.56	1	85.56	7.90	0.0376
A × C	162.56	1	162.56	15.00	0.0117
B × C	182.25	1	182.25	16.82	0.0093
A × A	0.9231	1	0.9231	0.0852	0.7821
B × B	4.67	1	4.67	0.4312	0.5404
C × C	9.75	1	9.75	0.8997	0.3864
Residual	54.19	5	10.84		
Lack of fit	17.69	3	5.90	0.3231	0.8135
Pure error	36.50	2	18.25		
Cor total	572.93	14			

of the plates. Figure 4 revealed that the interaction of electrode diameter and current in which UTS is increased due to increasing of electrode diameter and reduced by weld speed because more amount of material is transferred from the electrode to the joint during the process which reduces the gap and voids. Figure 5 illustrated the interaction of current and electrode diameter. This combination improves UTS when increasing both parameters' values. It is concluded that UTS is increasing by increasing electrode diameter and current and weld speed and decreasing by weld speed [42–45]. From ANOVA results that the combination of current and electrode diameters is the most influencing factor in the development of UTS. Similarly, Figs. 6, 7, and 8 show the interaction of all parameters on the response of hardness (Figs. 9, 10).

5 Optimization process

Box–Behnken optimization technique is a statistical experimental design method used to efficiently explore the response variables. It is particularly useful for optimizing complex systems where the relationship between input variables and the response is nonlinear. The advantages of the Box–Behnken optimization technique include its ability to efficiently explore the response surface, reduce the number of experimental runs required compared to a full factorial design, and capture important nonlinear effects. It is a valuable tool in process optimization, product development, and quality improvement, allowing for the identification of optimal operating conditions and the reduction of costs and time associated with experimentation. Finally, it allows for the identification of optimal factor levels and the understanding
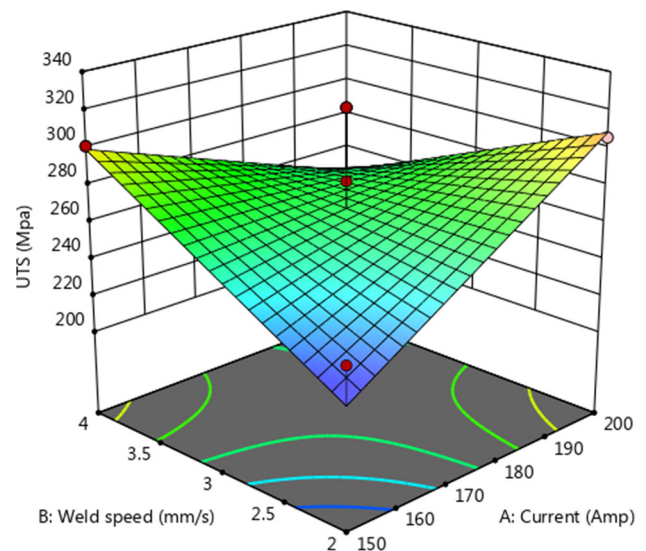
Fig. 4 Interaction between the welding speed and current

of the relationships between variables (current, weld speed, and electrode diameter) and the response (UTS and BHN). As per this Box–Behnken method, 15 experiments are conducted by combining three factors with three levels. The SN ratio for 15 experiments is computed using Minitab with lower conditions (small is better) as per Table 4. The SN ratio values of current, weld speed, and electrode diameter at each level for the response of Ultimate tensile strength and hardness are displayed in Figs. 11 and 12. By analyzing the signal-to-noise (S/N) ratio values, the optimal levels of each welding process parameter were determined, which corresponded to the highest values of the ultimate tensile strength
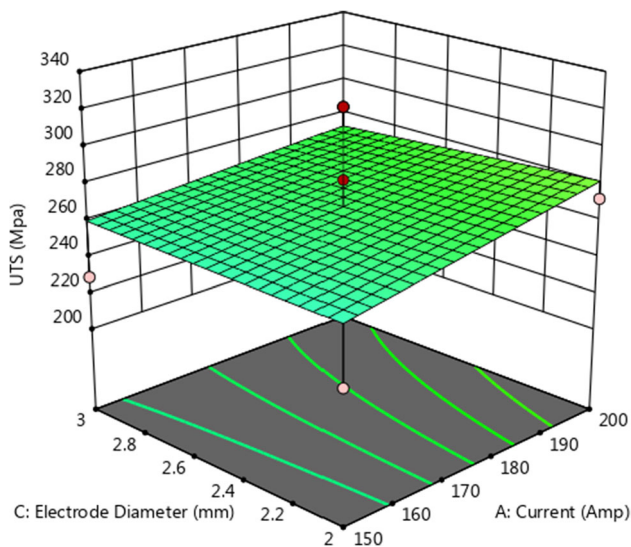
Fig. 5 Interaction between the electrode diameter and current
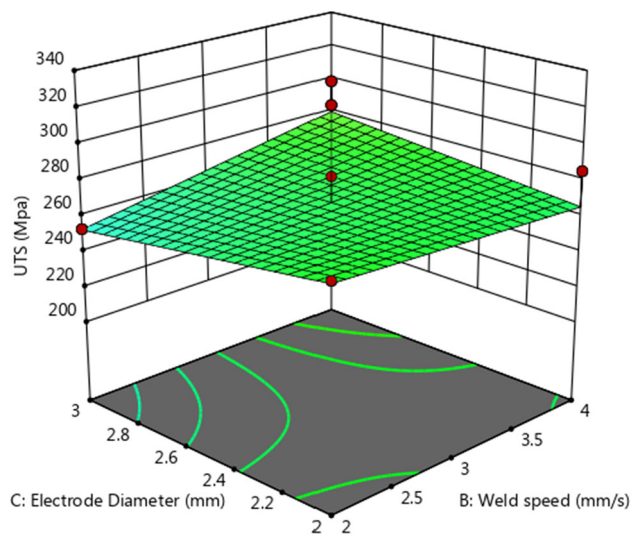

Fig. 6 Interaction between the electrode diameter and weld speed

(UTS) and Brinell hardness number (BHN). From Table 7 and Fig. 11, It is been observed that the optimal conditions for UTS are obtained at current-175 A (Level 2), welds speed-4 m/s (Level 3) and electrode diameter-2.5 mm (Level 2), it is noticed that higher UTS is attained when increasing current value. Similarly, from Table 8 and Fig. 12, the optimal condition of Hardness response at the current of 200 A (Level 3), weld speed of 4 m/s (Level 3), and electrode diameter of 3 mm (Level 3), and hardness values of the welding joint depend on the increasing current and weld speed.

Increasing the welding current (A) and weld speed (B) leads to an increase in ultimate tensile strength (UTS) due to higher heat production, which enhances the welding joint's mechanical properties. However, when the electrode diameter (C) is increased, UTS decreases as inadequate coalescence of the transferring filler material negatively affects the weld quality. Nevertheless, increasing welding current while decreasing welding speed can have adverse effects on welding quality. This results in a significant amount of spatter production, leading to some heat loss. Moreover, the weld nugget's columnar structure becomes coarser due to the higher heat input and reduced cooling rate, further compromising welding quality [46]. In contrast, Brinell Hardness Number (BHN) improves with increased welding current and speed, but it decreases with an increment in weld speed. This indicates that higher welding current and optimal welding speed contribute to improved hardness properties of the welded joint. However, excessively high weld speeds can negatively impact the BHN, potentially compromising the weld's mechanical integrity.

6 Microstructure analysis on fractured surfaces

The fracture surfaces of tensile samples can reveal important details about the impact of the joints' inherent microstructural characteristics on their strength. The fractured surfaces of the tensile test samples for Experiment-5 and Experiment-8 which analyzed by SEM. The random adequate porosity and shallow dimples with small size variation are disseminated on the fracture surface of Experiment no-5 and the depth and width of the observed dimples are more on the right side compared to other regions in Fig. 13a. It is also observed that there is deep void occurs at Experiment no: 8 which displayed in Fig. 13b. The void is present at weld pool due to absorption of oxygen and nitrogen from the atmosphere and also a poor provision of shielding gas. The main factor that leads to fracture is overload, and the coalescence of microporosity controls the failure. The regions near second-phase particle inclusions, the structure of grain, and displacement pileups are where the dimples may form. Therefore, as the strain increases during the tensile test, the micro gaps expand, combine, and ultimately create a continuous fracture surface.

The microstructures of all weld specimens consisted of the base austenite phase and the spread delta-ferrite phase. In the weld metal specimens under all conditions, ductile fracture was observed in the weld zone. The fracture was mainly located in the partially melted zone (PMZ) adjacent to the fusion boundary (FB) of the weld zone. This area combined different structures of original grains of γ-iron (un-melted), new grains of γ-iron or δ-iron (re-melted), and carbide precipitates. Each phase exhibited varying levels of hardness, with the carbide phase having the highest hardness compared to other phases. As a result, the zone became non-homogeneous
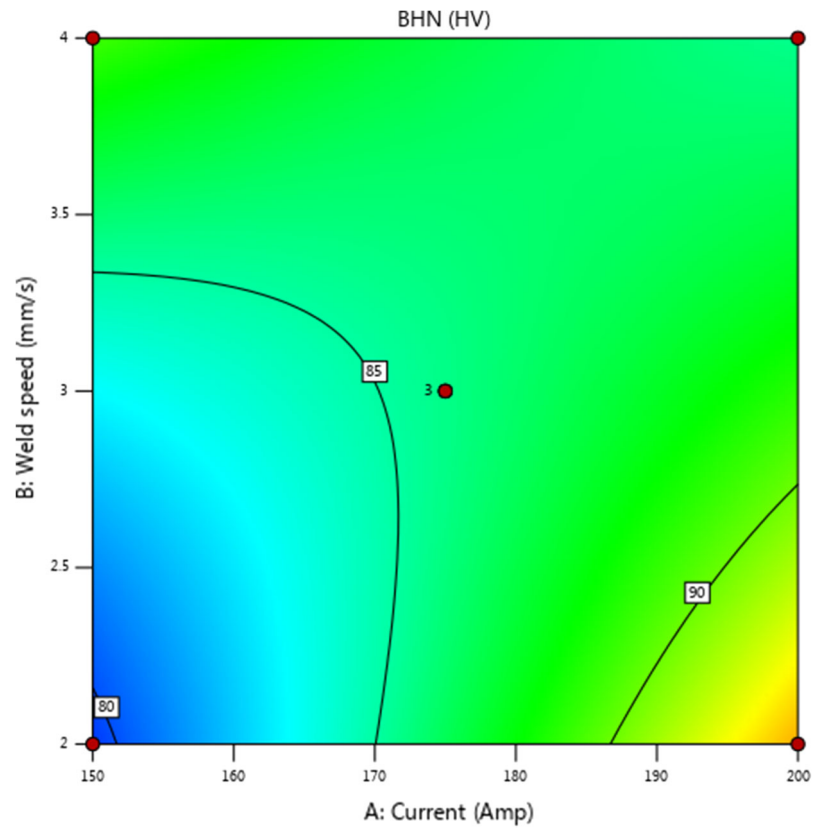
Fig. 7 Effect of weld speed and current on hardness

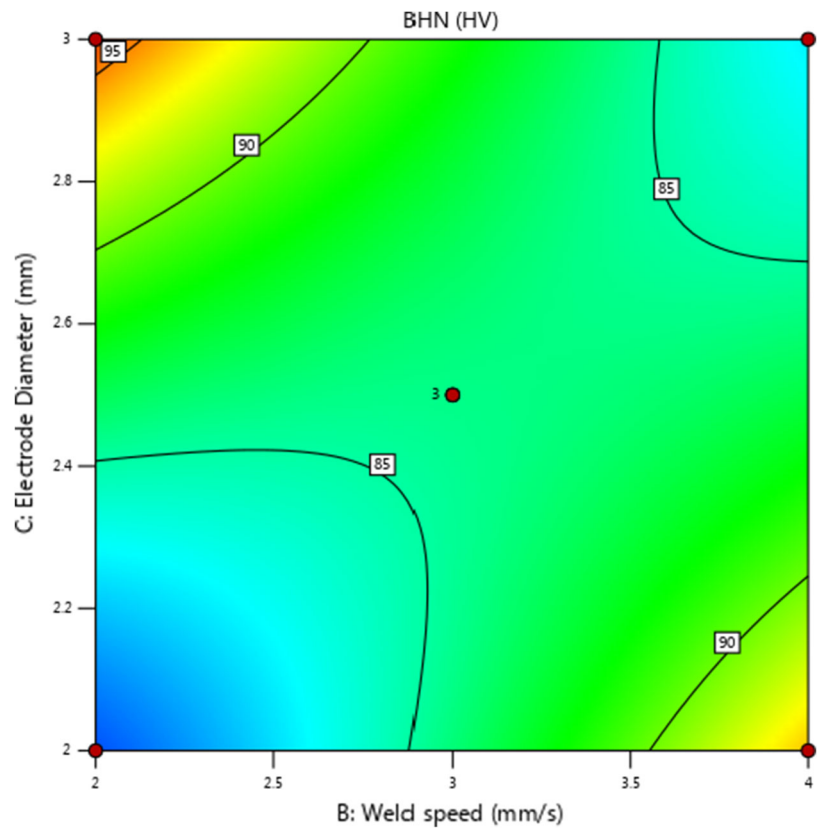**Fig. 8** Effect of weld speed and electrode diameter on hardness

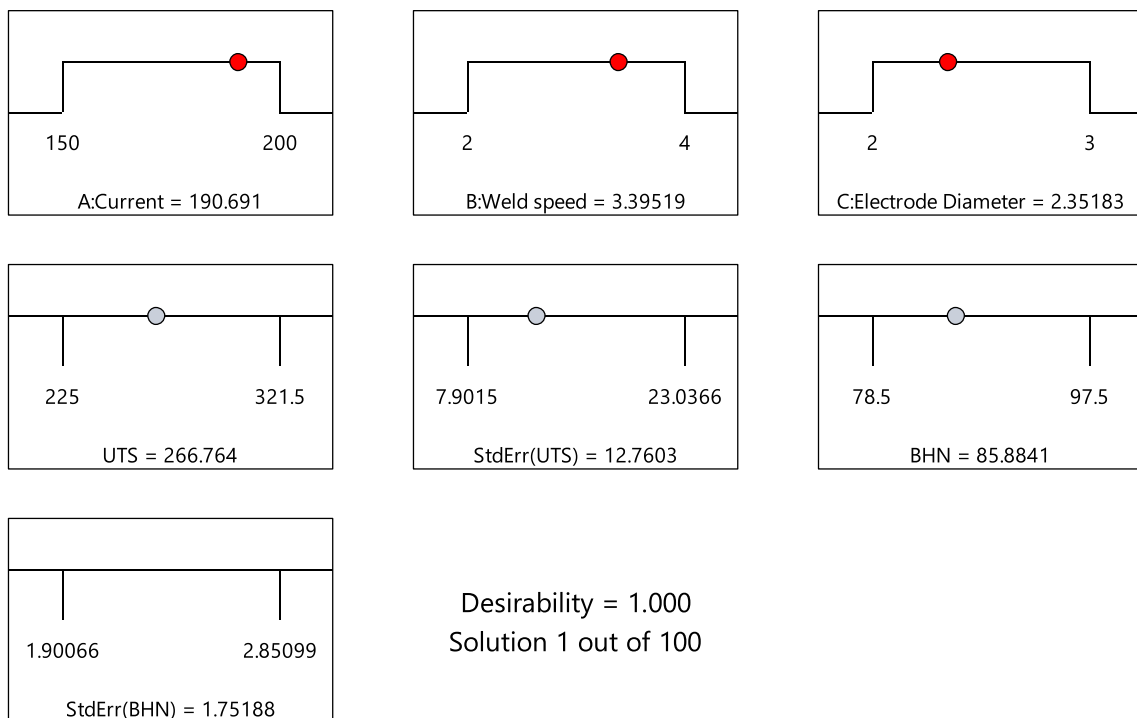**Fig. 9** Effect of current and electrode diameter on hardness

A:Current = 190.691
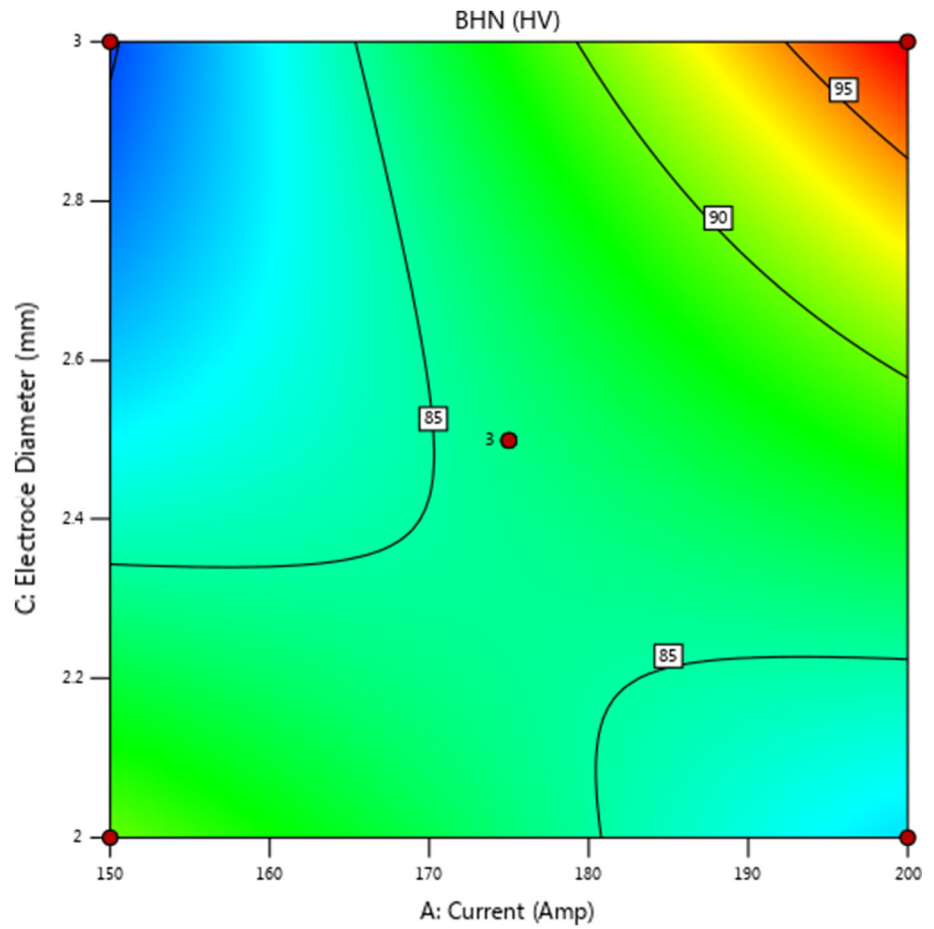
B:Weld speed = 3.39519

C:Electrode Diameter = 2.35183

UTS = 266.764

StdErr(UTS) = 12.7603

BHN = 85.8841

StdErr(BHN) = 1.75188

Desirability = 1.000
Solution 1 out of 100

Fig. 10 Predictions of tensile strength and HBN values for input considerations

Fig. 11 SN ratio plot for UTS

Main Effects Plot for SN ratios
Data Means

Signal-to-noise: Smaller is better

Fig. 12 SN ratio plot-BHN

Main Effects Plot for SN ratios
Data Means

Signal-to-noise: Smaller is better
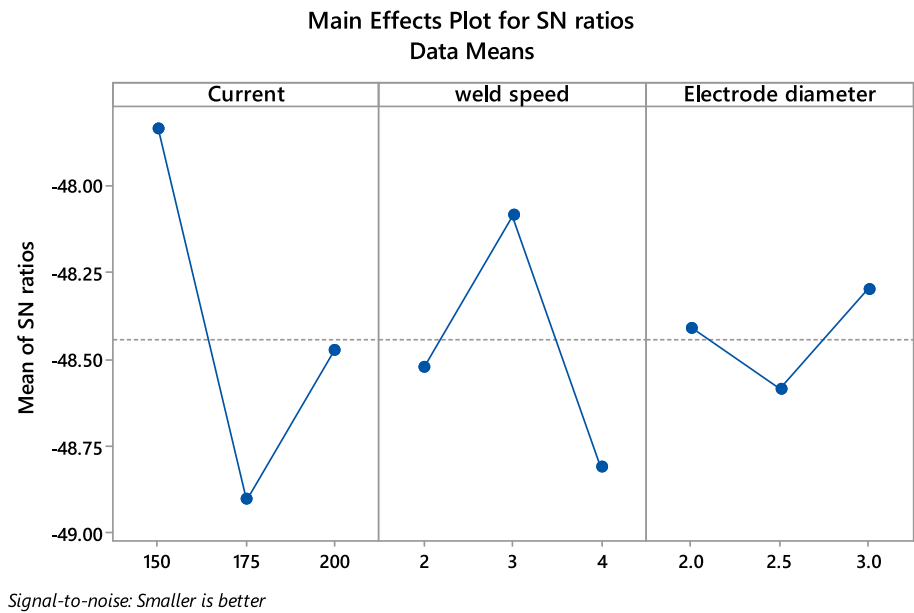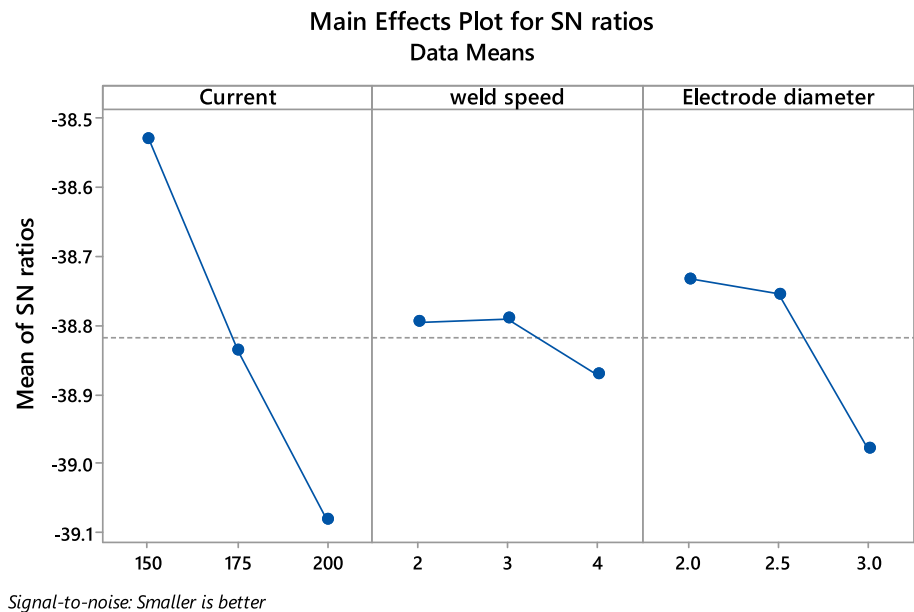
in properties, leading to reduced ductility and irregular deformation, which ultimately caused deep void to form in this area [3].

7 Conclusion

In this study, the Tungsten Inert Gas (TIG) welding process is used to join Chrome steels (EN31 and AISI52100), considering various process parameters such as current, weld speed, and electrode diameter. The primary objective is to investigate the impact of these TIG parameters on the tensile strength and hardness of the welded joints.

The Box–Behnken method is employed for the experimental design, leading to the fabrication of fifteen welded samples for evaluating the tensile and hardness properties. The key findings can be summarized as follows:

- The ultimate tensile strength and hardness values varied from 225 to 321.5 MPa and 78.5 to 97.5 HV, respectively. The optimal UTS was achieved with a current of 175 A, weld speed of 3 mm/min, and electrode diameter of 2.4 mm. On the other hand, the highest hardness was obtained with a current of 175 A, weld speed of 2 mm/min, and electrode diameter of 3 mm.

Table 7 Response table for UTS

Level	Current	Weld speed	Electrode diameter
1	− 47.84	− 48.52	− 48.41
2	− 48.91	− 48.09	− 48.59
3	− 48.47	− 48.81	− 48.30
Delta	1.07	0.72	0.29
Rank	1	2	3

Table 8 Response table for UTS

Level	Current	weld speed	Electrode diameter
1	− 38.53	− 38.80	− 38.73
2	− 38.84	− 38.79	− 38.76
3	− 39.08	− 38.87	− 38.98
Delta	0.55	0.08	0.25
Rank	1	3	2

Fig. 13 SEM image for **a** experiment-5 (150 A, 3 m/s, 2 mm), **b** experiment-8 (175 A, 3 m/s, 2.5 mm)
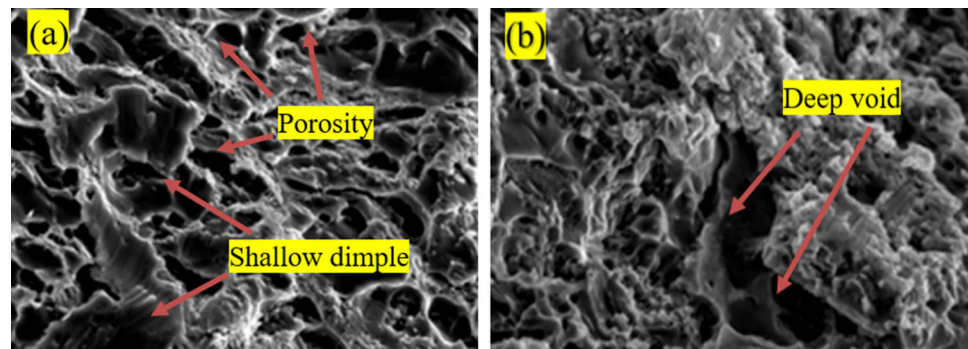
- Based on the signal-to-noise (SN) ratio analysis, the optimal parameters for achieving the highest tensile strength are identified as a current of 175 A, a weld speed of 4 m/s, and an electrode diameter of 2.5 mm.

 The ANOVA analysis indicated that the Fisher ratio value was less than 10, indicating the excellent fit of the ANOVA model for both tensile strength and hardness. Among the experimental parameters, the combination of current and welding speed was found to be the most significant factor in enhancing the mechanical properties of TIG welds.

- Tensile strength improves with increasing welding current and weld speed due to higher heat production. However, it decreases with an increase in electrode diameter because of inadequate coalescence of the transferring filler material. On the other hand, Brinell Hardness Number (BHN) improves with increased welding current and speed but decreases with a higher weld speed.
- The optimization results were obtained using a Box–Behnken ramp solution, resulting in the following values: ultimate tensile strength (UTS)—267 MPa and Brinell Hardness Number (BHN)—86 HV. These values were achieved with the following input factors: current of 191 A, weld speed of 3.4 mm/min, and electrode diameter of 2.35 mm. The corresponding standard errors for UTS and BHN were 12.7 and 1.75, respectively.
- The fractured surfaces of the tensile test samples from Experiment-5 and Experiment-8 were analyzed using Scanning Electron Microscopy (SEM). In Experiment-5, the SEM analysis revealed the presence of random, acceptable porosity, along with shallow dimples showing small size variation scattered on the fracture surface. The SEM analysis indicated that the depth and width of the observed dimples were more prominent on the right side compared to other regions in Experiment-8. Additionally, it was noticed that voids were present in the weld pool which could be attributed to the absorption of oxygen and nitrogen from the surrounding atmosphere, along with inadequate shielding gas provision during the welding process.

References

1. Balaram Naik, A., Chennakeshava Reddy, A.: Optimization of tensile strength in TIG welding using the Taguchi method and analysis of variance (ANOVA). Therm. Sci. Eng. Prog. **8**, 327–339 (2018). https://doi.org/10.1016/j.tsep.2018.08.005

2. Bodkhe, S.C., Dolas, D.R.: Optimization of activated tungsten inert gas welding of 304L austenitic stainless steel. Procedia Manuf. **20**, 277–282 (2018). https://doi.org/10.1016/j.promfg.2018.02.041

3. Chuaiphan, W., Srijaroenpramong, L.: Microstructure, mechanical properties and pitting corrosion of TIG weld joints alternative low-cost austenitic stainless steel grade 216. J. Adv. Join. Process. **2**(100027), 100027 (2020). https://doi.org/10.1016/j.jajp.2020.100027

4. Dadfar, M., Fathi, M.H., Karimzadeh, F., Dadfar, M.R., Saatchi, A.: Effect of TIG welding on corrosion behavior of 316L stainless steel. Mater. Lett. **61**(11–12), 2343–2346 (2007). https://doi.org/10.1016/j.matlet.2006.09.008

5. Kant, R., Dhami, S.S.: Multi-response optimization of parameters using GRA for abrasive water jet machining of EN31 steel. Mater. Today Proc. **47**, 6141–6146 (2021). https://doi.org/10.1016/j.matpr.2021.05.053

6. Kumar Sahu, A., Sivarajan, S., Padmanabhan, R.: Optimization of machining parameters in turning of EN31 steel with TiAlN coated cutting tool. Mater. Today Proc. **46**, 7497–7501 (2021). https://doi.org/10.1016/j.matpr.2021.01.180

7. Gugulothu, B., Satheesh Kumar, P.S., Srinivas, B., Ramakrishna, A., Vijayakumar, S.: Investigating the material removal rate parameters in ECM for Al 5086 alloy-reinforced silicon carbide/flyash hybrid composites by using Minitab-18. Adv. Mater. Sci. Eng. **2021**, 1–6 (2021). https://doi.org/10.1155/2021/2079811

8. Vijayakumar, S., Dhasarathan, N., Devabalan, P., Jehan, C.: Advancement and design of robotic manipulator control structures on cyber physical production system. J. Comput. Theor. Nanosci. **16**(2), 659–663 (2019). https://doi.org/10.1166/jctn.2019.7786

9. Venkata Ramana, M., Ravi Kumar, B.V.R., Krishna, M., Venkateshwar Rao, M., Kumar, V.S.: Optimization and influence of process parameters of dissimilar SS304L–SS430 joints produced by robotic TIG welding. Mater. Today Proc. **23**, 479–482 (2020). https://doi.org/10.1016/j.matpr.2019.05.388

10. Paramasivam, P., Vijayakumar, S.: Mechanical characterization of aluminium alloy 6063 using destructive and non-destructive testing. Mater. Today Proc. **81**, 965–968 (2023). https://doi.org/10.1016/j.matpr.2021.04.312

11. Anusha, P., Sri, M.N.S., Vijayakumar, S., Rao, T.V.J., Paramasivam, P., Jeyakrishnan, S., Saxena, K.K.: Design and optimization the wear characteristics for Al7178/TiO2/B4C/FA central hybrid composite. Int. J. Interact. Des. Manuf. (IJIDeM) (2023). https://doi.org/10.1007/s12008-023-01341-5

12. Gugulothu, B., Bharadwaja, K., Vijayakumar, S., Rao, T.V.J., Sri, M.N.S., Anusha, P., Agrawal, M.K.: Modeling and parametric optimization of electrical discharge machining on casted composite using central composite design. Int. J. Interact. Des. Manuf. (IJIDeM) (2023). https://doi.org/10.1007/s12008-023-01323-7

13. Rajput, S.K., Kumar, J., Mehta, Y., Soota, T., Saxena, K.K.: Microstructural evolution and mechanical properties of 316L stainless steel using multiaxial forging. Adv. Mater. Process. Technol. **6**(3), 509–518 (2020). https://doi.org/10.1080/2374068x.2020.1728641

14. Pydi, H.P., Pasupulla, A.P., Vijayakumar, S., Agisho, H.A.: Study on microstructure, behavior and Al$_2$O3 content flux A-TIG weldment of SS-316L steel. Mater. Today Proc. **51**, 728–734 (2022). https://doi.org/10.1016/j.matpr.2021.06.218

15. Samyal, R., Bagha, A.K., Bedi, R., Bahl, S., Saxena, K.K., Sehgal, S.: Predicting the effect of fiber orientations and boundary conditions on the optimal placement of PZT sensor on the composite structures. Mater. Res. Express **8**(7), 075302 (2021). https://doi.org/10.1088/2053-1591/ac0de9

16. Wang, Y., Cong, B., Qi, B., Yang, M., Lin, S.: Process characteristics and properties of AA2219 aluminum alloy welded by double pulsed VPTIG welding. J. Mater. Process. Technol. **266**, 255–263 (2019). https://doi.org/10.1016/j.jmatprotec.2018.11.015

17. Saxena, K.K., Pancholi, V., Jha, S.K., Chaudhari, G.P., Srivastava, D., Dey, G.K.: A novel approach to understand the deformation behavior in two phase region using processing map. J. Alloys Compd. **706**, 511–519 (2017). https://doi.org/10.1016/j.jallcom.2017.02.177

18. Sankar, V.V.A., Suresh, P., Sridharan, P., Vignesh, R., Gowtham, M.: Mathematical and MATLAB based process optimization by simulated annealing algorithm for wire electrical discharge machining of EN31. Mater. Today Proc. **47**, 6941–6946 (2021). https://doi.org/10.1016/j.matpr.2021.05.209

19. Vinoth, V., Sudalaimani, R., Veera Ajay, C., Suresh Kumar, C., Sanjeevi Prakash, K.: Optimization of mechanical behaviour of TIG welded 316 stainless steel using Taguchi based grey relational analysis method. Mater. Today Proc. **45**, 7986–7993 (2021). https://doi.org/10.1016/j.matpr.2020.12.1002

20. Upadhyay, S., Saxena, K.K.: Effect of Cu and Mo addition on mechanical properties and microstructure of grey cast iron: an overview. Mater. Today Proc. **26**, 2462–2470 (2020). https://doi.org/10.1016/j.matpr.2020.02.524

21. Bahl, S., Singh, T., Kumar, V., Sehgal, S., Bagha, A.K.: A systematic review on recent progress in advanced joining techniques of the lightweight materials. AIMS Mater. Sci. **8**(1), 62–81 (2021)

22. Natrayan, L., Anand, R., Santhosh Kumar, S.: Optimization of process parameters in TIG welding of AISI 4140 stainless steel using Taguchi technique. Mater. Today Proc. **37**, 1550–1553 (2021). https://doi.org/10.1016/j.matpr.2020.07.150

23. Sharma, A., Sehgal, S., Goyal, D.: Effects of process parameters in joining of Inconel-625 alloy through microwave hybrid heating. Mater. Today Proc. **28**, 1323–1327 (2020). https://doi.org/10.1016/j.matpr.2020.04.590

24. Sekhon, S.S., Kumar, H., Sehgal, S.: Effect of tool pin profile on performance of friction stir welding of brass-copper-based butt welded joint. Int. J. Mater. Eng. Innov. **7**(3/4), 236 (2016). https://doi.org/10.1504/ijmatei.2016.084627

25. Shanmugasundar, G., Karthikeyan, B., Ponvell, P.S., Vignesh, V.: Optimization of process parameters in TIG welded joints of AISI 304L -austenitic stainless steel using Taguchi's experimental design method. Mater. Today Proc. **16**, 1188–1195 (2019). https://doi.org/10.1016/j.matpr.2019.05.213

26. Wan, Z., Meng, D., Zhao, Y., Zhang, D., Wang, Q., Shan, J., Song, J., Wang, G., Wu, A.: Improvement on the tensile properties of 2219-T8 aluminum alloy TIG welding joint with weld geometry optimization. J. Manuf. Process. **67**, 275–285 (2021). https://doi.org/10.1016/j.jmapro.2021.04.062

27. Kumar, P.S.S., Allamraju, K.V.: A review of natural fiber composites [jute, sisal, Kenaf]. Mater. Today Proc. **18**, 2556–2562 (2019). https://doi.org/10.1016/j.matpr.2019.07.113

28. Budarapu, P.R., Sastry, S., Natarajan, R.: Design concepts of an aircraft wing: composite and morphing airfoil with auxetic structures. Front. Struct. Civ. Eng. **10**(4), 394–408 (2016). https://doi.org/10.1007/s11709-016-0352-z

29. Budarapu, P.R., Yb, S.S., Javvaji, B., Mahapatra, D.R.: Vibration analysis of multi-walled carbon nanotubes embedded in elastic medium. Front. Struct. Civ. Eng. **8**(2), 151–159 (2014). https://doi.org/10.1007/s11709-014-0247-9

30. Jaffery, H.A., Sabri, M.F.M., Said, S.M., Hasan, S.W., Sajid, I.H., Nordin, N.I.M., Megat Hasnan, M.M.I., Shnawah, D.A.,

Moorthy, C.V.: Electrochemical corrosion behavior of Sn–0.7Cu solder alloy with the addition of bismuth and iron. J. Alloys Compd. **810**(151925), 151925 (2019). https://doi.org/10.1016/j.jallcom.2019.151925

31. Guoqing, W., Quan, Li., Yanjun, Li., et al.: Effects of weld reinforcement on tensile behavior and mechanical properties of 2219-T87 aluminum alloy TIG welded joints. Trans. Nonferrous Metals Soc. China **27**(1), 10–16 (2017)

32. Vijayakumar, S., Arunkumar, A., Pradeep, A., Satishkumar, P., Singh, B., Rama Raju, K.S., Sharma, V.K.: Optimization of process variables for shielded metal arc welding dissimilar mild steel and medium carbon steel joints. J. Adhes. Sci. Technol. (2023). https://doi.org/10.1080/01694243.2023.2227461

33. Dhawan, A., Gupta, N., Goyal, R., Saxena, K.K.: Evaluation of mechanical properties of concrete manufactured with fly ash, bagasse ash and banana fibre. Mater. Today Proc. **44**, 17–22 (2021). https://doi.org/10.1016/j.matpr.2020.06.006

34. Gupta, N., Gupta, A., Saxena, K.K., Shukla, A., Goyal, S.K.: Mechanical and durability properties of geopolymer concrete composite at varying superplasticizer dosage. Mater. Today Proc. **44**, 12–16 (2021). https://doi.org/10.1016/j.matpr.2020.05.646

35. Kumar, N., Bharti, A., Saxena, K.K.: A re-investigation: effect of powder metallurgy parameters on the physical and mechanical properties of aluminium matrix composites. Mater. Today Proc. **44**, 2188–2193 (2021). https://doi.org/10.1016/j.matpr.2020.12.351

36. Grayeli Korpi, A., Ţălu, Ş, Bramowicz, M., Arman, A., Kulesza, S., Pszczolkowski, B., Jurečka, S., Mardani, M., Luna, C., Balashabadi, P., Rezaee, S., Gopikishan, S.: Minkowski functional characterization and fractal analysis of surfaces of titanium nitride films. Mater. Res. Express **6**(8), 086463 (2019). https://doi.org/10.1088/2053-1591/ab26be

37. Yadav, S., Sharma, P., Yamasani, P., Minaev, S., Kumar, S.: A prototype micro-thermoelectric power generator for micro-electromechanical systems. Appl. Phys. Lett. (2014). https://doi.org/10.1063/1.4870260

38. Gupta, T.K., Budarapu, P.R., Chappidi, S.R., Sastry, S., Paggi, M., Bordas, S.P.: Advances in carbon based nanomaterials for bio-medical applications. Curr. Med. Chem. **26**(38), 6851–6877 (2019). https://doi.org/10.2174/0929867326666181126113605

39. Krishnaja, D., Cheepu, M., Venkateswarlu, D.: A review of research progress on dissimilar laser weld-brazing of automotive applications. IOP Conf. Ser. Mater. Sci. Eng. **330**, 012073 (2018). https://doi.org/10.1088/1757-899x/330/1/012073

40. Balguri, P.K., Samuel, D.G.H., Thumu, U.: A review on mechanical properties of epoxy nanocomposites. Mater. Today Proc. **44**, 346–355 (2021). https://doi.org/10.1016/j.matpr.2020.09.742

41. SudhirSastry, Y.B., Krishna, Y., Budarapu, P.R.: Parametric studies on buckling of thin walled channel beams. Comput. Mater. Sci. **96**, 416–424 (2015). https://doi.org/10.1016/j.commatsci.2014.07.058

42. Manickam, S., Pradeep, A., Vijayakumar, S., Mosisa, E.: Optimization of arc welding process parameters for joining dissimilar metals. Mater. Today Proc. (2022). https://doi.org/10.1016/j.matpr.2022.06.548

43. Pradeep, A., Kavitha, N., Janardhana Rao, T.V., Vijayakumar, S.: Influence of nano alumina/vegetable oil based cutting fluid on MQL turning of stainless steel 304. Mater. Today Proc. (2022). https://doi.org/10.1016/j.matpr.2022.06.547

44. Vijayakumar, S., Anitha, S., Arivazhagan, R., Hailu, A.D., Rao, T.V.J., Pydi, H.P.: Wear investigation of aluminum alloy surface layers fabricated through friction stir welding method. Adv. Mater. Sci. Eng. **2022**, 1–8 (2022). https://doi.org/10.1155/2022/4120145

45. Vijayakumar, S., Manickam, S., Seetharaman, S., Rao, T.V.J., Pounraj, D., Pydi, H.P.: Examination of friction stir-welded AA 6262/5456 joints through the optimization technique. Adv. Mater. Sci. Eng. **2022**, 1–11 (2022). https://doi.org/10.1155/2022/4527595

46. Zhang, X., Yao, F., Ren, Z., Yu, H.: Effect of welding current on weld formation, microstructure, and mechanical properties in resistance spot welding of CR590T/340Y galvanized dual phase steel. Materials **11**(11), 2310 (2018). https://doi.org/10.3390/ma11112310